Micromechanical Properties of the Interphase in Cellulose Nanofiber-reinforced Phenol Formaldehyde Bondlines

Cong Liu,[a,b] Yang Zhang,[a] Siqun Wang,[b,*] Yujie Meng,[b] and Omid Hosseinaei [b]

Lab-processed cellulose nanofibrils (CNF-L), commercial cellulose nanofibrils (CNF-C), and cellulose nanocrystals (CNC) were used in this study as reinforcing materials in phenol formaldehyde (PF) resin. The mechanical modification of adhesives and cell wall layers (S2 and compound corner-middle lamellae [CCML]) by the three types of cellulose particles was investigated by nanoindentation. Results showed that cellulose nano-materials can improve the mechanical properties of both adhesives and the cell wall structure. CNF-C had the most obvious reinforcing effect on the elastic modulus (E_r) and hardness within the glue line. With modification, the E_r and hardness reached 13.0 and 0.436 GPa, respectively, in the S2 layer far from the glue line. In comparison, the control sample had an E_r and hardness of 7.31 and 0.256 GPa, respectively.

Contact information: a: College of Materials Science and Engineering, Nanjing Forestry University, Nanjing 210037, PR China; b: Center for Renewable Carbon, University of Tennessee, Knoxville, TN 37996, USA;
* Corresponding author: swang@utk.edu

INTRODUCTION

The chemical properties, wettability, adhesive distribution, and adhesive penetration of adhesives are the primary factors influencing wood composite performance (Stöckel *et al.* 2010). As a result, the choice of adhesive has a great influence on the performance of the composite. Phenol formaldehyde (PF) resin is a thermal-setting resin that has been used for over 100 years (Dong *et al.* 2009). PF resin performs well with respect to adhesive strength, water resistance, heat resistance, wear resistance, and chemical stability. However, despite these advantages, some characteristics exhibit room for improvement.

There are several theories about the bonding mechanism of adhesives (Marra 1992; Pizzi 1994; Gindl *et al.* 2004; Obersriebnig 2011). One, the absorption or thermodynamic theory, posits interatomic forces as the foundation for adhesion. Another, the mechanical interlocking theory, assumes interlocking of the surface structures as a contributor to adhesion strength. The electronic theory suggests an electron transfer between substrate and adhesive as the cause of adhesion. A fourth theory involves chemical bonds, which have a considerably higher bond strength (100 to 1000 kJ/mol) than the non-covalent van der Waals and hydrogen bonds (less than 50 kJ/mol), acting as a bridge between a substrate and an adhesive that normally would not bond well. In the theory of boundary layers and interphases, the formation of interphases (ranging in size between a few angstroms to several micrometers) is considered when analyzing an adhesive bond, as the interphase can

greatly influence the properties of the bond. The diffusion theory assumes the mutual diffusion of macromolecules across an adhesively bonded interface as a mechanism of adhesion (Marra 1992). Several studies have shown that certain wood adhesives infiltrate wood cell walls and thus can potentially change cell-wall properties (Konnerth *et al.* 2007; Jakes *et al.* 2009; Liang *et al.* 2011; Obeng *et al.* 2013). Furthermore, the penetration of PF resin into cells (cell walls and lumens) is confirmed to form wood and glue compounds (Gindl *et al.* 2004; Hunt *et al.* 2010). In addition, PF resin penetration creates greater bond stability with respect to resistance to hydrolysis, durability over time, and mechanical stability of bond-lines.

Although PF resin is moisture-resistant and has acceptable strength properties, its mechanical properties can further be improved by reinforcement. The synthetic composite material of which bondlines are composed is usually on the order of micrometers and greater, creating the adhesive as its own phase. Adhesive systems for these materials often create a distinct interface on the micron scale, with 2 to 10% of the total weight composed of particulate and laminate composites and more than half of the material composed of fiber-reinforced thermoplastic composites. Reducing adhesive consumption and combining dissimilar materials to a single adhesive system are challenging issues, which if resolved have the potential to increase composite performance and reduce costs (Zhou *et al.* 2010). Therefore, reinforcing the adhesive bondline with cellulose nanomaterials is an intelligent solution.

The composition and composite structure of cells are different in different cell-wall layers. Of the S1, S2, and S3 layers, the S2 layer is the thickest layer of the secondary wall and consists of about 35% highly oriented semi-crystalline cellulose microfibrils embedded in a matrix of 20% amorphous cellulose, 30% hemicellulose, and 15% lignin (Liang *et al.* 2011). When applied in nano-scale, CNF as a biopolymer show outstanding mechanical properties. The crystalline part of cellulose has an estimated strength of up to 10GPa and an elastic modulus of 138 GPa (Veigel *et al.* 2011). Even when taking the paracrystalline regions and material degradation during processing into consideration, the low density cellulose is still competitive compared to synthetic fiber materials. Konnerth and Gindl (2006) bonded spruce wood (*Picea abies*) with phenol–resorcinol–formaldehyde adhesive (PRF) and found that wood cell walls exhibited the highest elastic modulus, from 12 to 24 GPa, while the cured PRF adhesive's elastic modulus was around 7 GPa. The elastic modulus of the adhesive was clearly lower than the modulus of the wood cell walls. Therefore, adhesive reinforcement is necessary, although it may hinder the composite fracture in the bondline.

There have been several studies aimed at improving the mechanical properties of wood adhesives by reinforcing the adhesives with nanoparticles (Kaboorani *et al.* 2012; Salari *et al.* 2012) or CNFs (Wang and Xing 2010; Veigel *et al.* 2011; Atta-Obeng *et al.* 2013). Our own investigation (Wang and Xing 2010) has shown that oriented strand board (OSB) properties can be improved by reinforcing the glueline strength, preventing phenol-formaldehyde (PF) resin from penetrating into wood pores, and increasing resin coverage on the strand surface. Three to four percent of nano-material filler is enough to improve resin performance and OSB properties. When 3% of CNF (based on the oven-dried weight of resin) was added, the elastic modulus of resin increased 31.6% and strength increased 24.1% (from 79 MPa to 98 MPa). The modulus of OSB panels increased 12.1% to 3605 MPa with the addition of 4% CNF into the resin (based on the oven-dried weight of resin). In addition, the bending strength increased 14.5% to 30.8 MPa. Another key factor, internal bond strength, increased as well. However, the thickness swelling (TS) decreased. In a

2012 study, Salari *et al.* (2012) applied low-quality paulownia wood oriented strand board (OSB) to study the effect of nanoclay on the wood. Although none of the panels satisfied the thickness swelling and water absorption requirements, the results of the X-ray diffraction and transmission electron microscope analysis confirmed a thorough dispersion of nanoclay in the resulting OSBs. By increasing the proportion of nanoclay to urea-formaldehyde (UF) resin to 5%, the mechanical and physical properties of the resulting panels were improved and formaldehyde emissions decreased. Obeng *et al.* (2013) dispersed micro-sized crystalline cellulose at loadings of 0, 3, 6, and 10% (by weight) in PF and tested the thermal properties and shear strength. At the conclusion of the study, an increase in composite strength was found. The heat of the reaction and nonlinear behavior in lap shear strength with cellulose loading suggests an interaction between the cellulose and the PF polymer that appears to have been optimized at 3% cellulose loading.

To investigate the effect of added cellulose filler on the fracture properties of wood adhesive bonds, double cantilever beam specimens were prepared from spruce wood (Veigel *et al.* 2011). While the highest fracture energy values were observed in UF bonds filled with untreated nanofibrils prepared from wood pulp, bonds filled with TEMPO-oxidized fibrils showed less satisfying performance. It is proposed that UF-adhesive bonds can be significantly toughened by the addition of miniscule amounts of cellulose nanofibrils. The optimum filler content is largely dependent on the adhesive and the type of cellulose filler used.

However, the distribution of nano materials across the bondline is still unknown. The objective of this research was to investigate, by means of nanoindentation, the effect of cellulose nanomaterials (CNF-L, CNF-C, and CNC) on the mechanical properties of the interphase in reinforced bondlines.

EXPERIMENTAL

Materials

Red oak samples were obtained from the discs of 45-year-old trees (counted from pith to bark) in Knoxville, TN. The samples had an average density of 0.716 g/cm^3, microfibril angle (MFA) of 10.4°, and an elastic modulus (MOE) reading of 16 GPa. All the density, MFA, and MOE figures were obtained from a SilviScan Analysis of two hardwood species at the Pulp and Paper Research Institute of Canada (Wu *et al.* 2009). SilviScan is an instrument for efficient measurement of many wood and fibre properties of importance for both research and industry, such as wood density, wood stiffness, fibre dimensions, microfibril angle, annual rings, and wood stiffness. The SilviScan integrates three measurement principles: image analysis of fibre cross-sections, x-ray absorption, and X-ray diffraction of wood, performed along radii from pith to bark. The SilviScan system was from EvalueTree Technical Corp (Vancouver, Canada) at the Pulp and Paper Research Institute of Canada (Paprican, UBC Campus, Vancouver, BC, Canada). Density was scanned at a resolution of 25 mm, whereas MFA was in a resolution of 1 mm. Phenolic resin (PF) was procured from the Arclin Corporation (Mississauga, Ontario, Canada). Its non-volatile solids content was 44.5 to 45.45%, its viscosity was 40 to 90 cps, and its pH was 10.3 to 10.7.

Three types of cellulose microfibers were used as reinforced materials in this research. Cellulose nanofibrils (CNF-L), using cellulose particles (Creafill Inc., Chestertown, MD) as a raw material, was processed at the National Institute of Advanced

Industrial Science and Technology (AIST) in Japan. The 3% cellulose suspension was processed into nanofibers using an ultrafine grinder (Masuko Sangyo Co., Japan) following a previously described procedure (Jang *et al.* 2013; Lee *et al.* 2010 and 2013; Teixeira *et al.* 2013). The grinder consisted of lower rotating and upper stationary SiC grinding stones (gap 100 μm), and the cellulose suspension was recirculated into the grinder five times. Water was added during the grinding process, resulting in a nanocellulose with a solid content of 1.3%. Contamination from the grinding stones was assumed to be negligible. The length is represented in micrometers, and all diameters were less than 100 nm, as shown in Fig. 1a. The CNF-L water suspension was centrifuged to result in a hydrogel with a final solid content of 5%. Commercial cellulose nanofibril (CNF -C) was purchased from Intelligent Chemicals, Ltd. (Wuxi, Jiangsu, China) and used directly, with 10% solid content; the fibers' average length was in the range of 400 to 600 μm, and the average diameter was in the range of 10 to 50 nm. The size and structure are shown in Fig. 1b. The switchgrass cellulose nanocrystals (CNC) were selected to represent CNC due to its high aspect ratio (Meng *et al.* 2014). The CNC were prepared from switchgrass cellulose powder with sulfuric acid. The disordered or paracrystalline regions of the cellulose were preferentially hydrolyzed, whereas the crystalline regions, which had a higher resistance to acid attack, remained intact. The procedure has been described in detail in a previous publication (Wu *et al.* 2013). The resulting suspension was subsequently diluted with water and washed with successive centrifugations. Dialysis against distilled water was then performed to remove any free acid molecules from the dispersion. Additional steps, such as ultrasonication, were performed to achieve the suspension. The average particle diameter was approximately 3.9 nm, and the average length was 148 nm (Wu *et al.* 2013). The CNC was freeze-dried before mixed with PF resin.
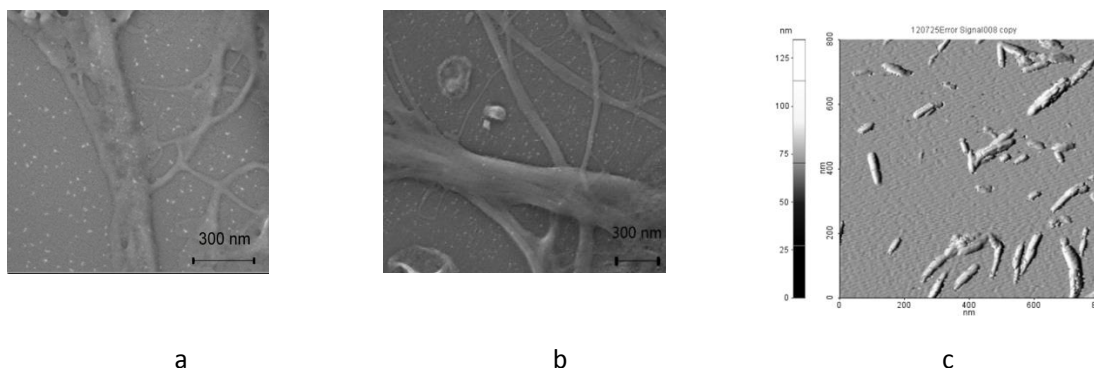

a   b   c

Fig. 1. Images of three kinds of cellulose particles: (a) SEM image of CNF-L, (b) SEM image of CNF-C, and (c) AFM image of CNC

Methods

Morphology measurements

A scanning electron microscope (Zeiss Dual Beam SEM instrument, Germany) was used to characterize the morphology of MFC-L and MFC-C. The samples were prepared by depositing a drop of suspension with concentration of 0.001 wt% onto freshly cleaved mica, and then were oven dried at 45 °C until all the water was removed. The films on mica could be observed by SEM.

Atomic force microscopy (AFM) (XE-100, PSIA, Korea) was used to characterize the morphology of switchgrass CNC in the noncontact mode. The error signal image was attained by 10 silicon AFM probes, with tip height 14 μm and radius < 10 nm. The spring

constant was 40 N/m and resonant frequency 300 kHz. The samples were prepared by depositing a drop of CNC suspension with concentration of 0.01 wt% onto freshly cleaved mica, and then were dried to remove all the water. The CNC films were observed by AFM.

Sample preparation

The samples were prepared from the same growth ring of red oak (specifically the 35th growth ring, MFA10.7). The sample length was parallel to the grain direction and perpendicular to the growth ring. Samples were then cut into the following size: 2 (T) x 2 (R) x 5 (L) cm. The samples were divided into four groups; the controls were treated with PF resin, while the rest were processed with PF resin to which different cellulose particles (CNF-L, CNF-C and CNC) had been added. And each group had three glued samples to represent each condition.

Three percent of either CNF-L, CNF-C, or CNC was added to the PF resin, in accordance with the solid content ratio. The PF resin was spread on one face of the sample at 160 g/m^2 (single-face), and the tangential and radial surfaces were then bonded together. The glued samples were cured at 160 °C for 30 min in an oven. The bonded samples were cut with a microtome in a pyramidal fashion following the procedure described in a previous publication (Meng *et al.* 2013). The PF resins with cellulose nanomaterials were also cured at 160 °C for 30 min in an oven for nanoindentation evaluation.

Each specimen was then mounted on an ultramicrotome, and a cross section was cut with a glass knife. Finally, the specimen surface was cut with a diamond knife to obtain a smoother surface. The smoothed specimens were conditioned in the nanoindentation test room for at least 24 h at 21± 1°C and 60 ±5% relative humidity (RH) before the nanoindentation was performed.

Nanoindentation procedure

A Triboindenter (Hysitron Inc., Minneapolis, MN) equipped with a diamond Berkovichtip that was operated in an open-loop control was used for the nanoindentation. The test was conducted on the wood's secondary wall (S2 layer), compound corner-middle lamellae (CCML), the adhesive interior lumen, and glue lines at three typical locations in the bondline (Fig. 2). The first location was in the glue line and was conducted in a manner so that only the adhesive was indented.
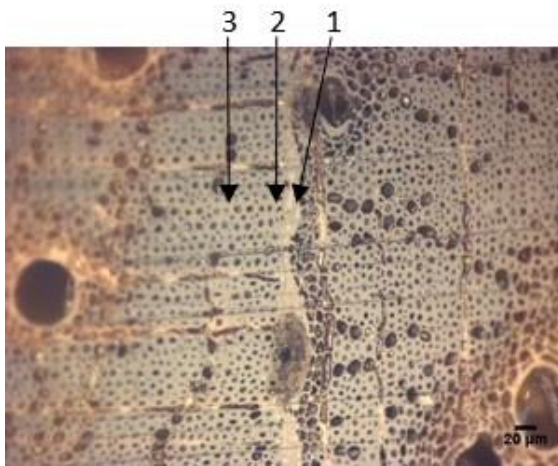

Fig. 2. Nanoindentation positions-optics microscope: (1) in the glue line; (2) one or two cells away from the glue line; and (3) far from the glue line

The second location was just one or two wood cells away from the glue line, at which all of the lumens were filled with PF resin. The third location was far from the glue line and varied due to the large variation of PF resin penetration depth. Wood cells filled with adhesive were chosen for nanoindentation. The hardness (H) and elastic modulus (E_r) with and without cellulose particle additives in the adhesive were tested at very small scales to assess the effect of cellulose nanoparticle additives on these properties.

As shown below in Fig. 3a, the load function contained three stages: the loading stage (increasing from 0 to 250 µN for 5 min), the holding load stage (keeping the load at 250 µN for 5 min), and the unloading stage (decreasing from 250 to 0 µN for 5 min). The total nanoindentation procedure took 15 min. Figure 3b shows the instantaneous elastic deformation during the first stage; during the second, under maximum load, the displacement increases. When the load is withdrawn at constant speed, some of the deformation recovers, but some remains as a permanent deformation known as plastic deformation. The permanent deformation is described as a triangle pit by Yan and Li (2013).
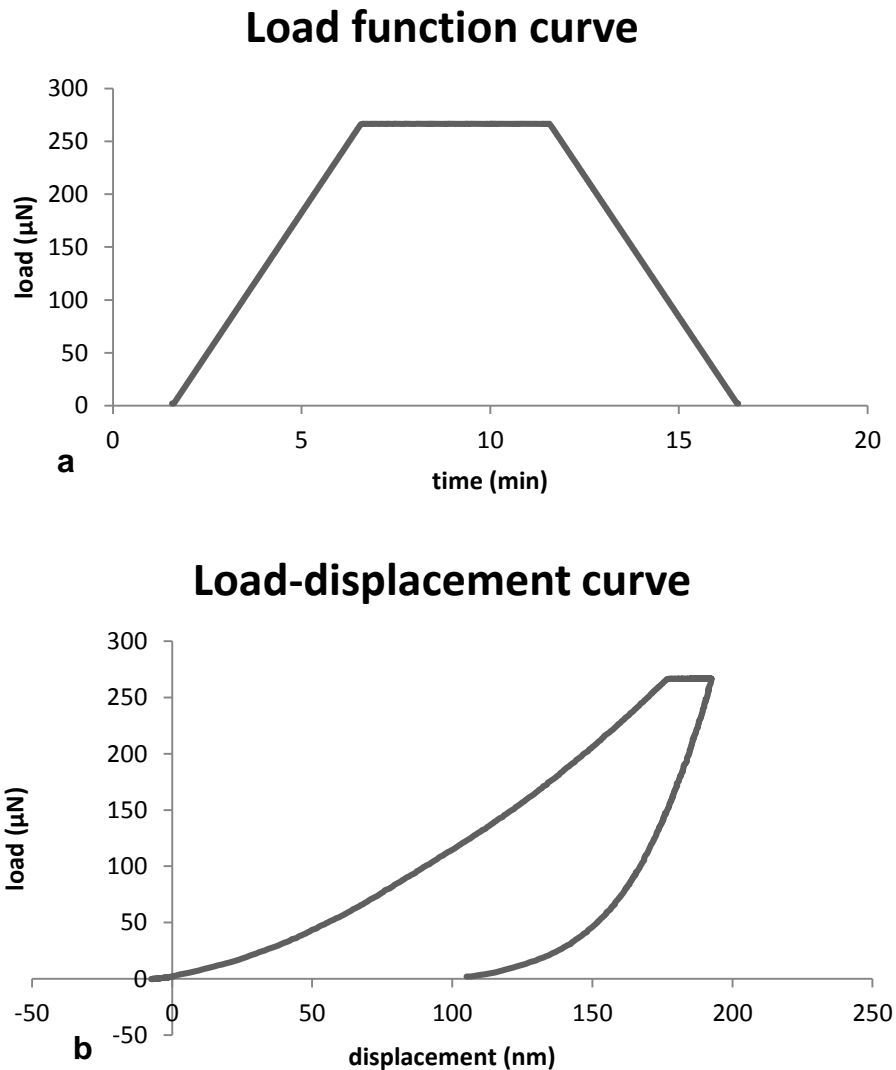
Load function curve

a

Load-displacement curve

b

Fig. 3. Load and time parameters: (a) load function curve; (b) load-displacement curve

Values of H and E_r were calculated from the load–displacement data shown in Fig. 3b. As the indenter penetrated into the specimen, both elastic and plastic deformation occurred, and only the elastic portion of the displacement recovered during unloading.

Nanoindentation hardness is defined as follows (Oliver and Pharr 1992; Konnerth *et al.* 2007; Liang *et al.* 2011),

$$H = \frac{Pmax}{A} = \frac{Pmax}{24.5hc^2} \tag{1}$$

where P_{max} is the load measured at a maximum depth of penetration (h) in an indentation cycle, A is the projected contact area, and h_c is the contact depth of the indentation, given by:

$$h_c = h - 0.75\frac{Pmax}{S} \tag{2}$$

where S is the slope ($\frac{\mathrm{dp}}{\mathrm{dh}}$) of the initial portion of the unloading curve at $h = h_{max}$ and 0.75 is a constant that is dependent on the indenter geometry.

The specimen's reduced modulus (E_r) can be obtained using the following equation,

$$E_r = \frac{\sqrt{\pi}}{2\sqrt{A(h_c)}} \cdot S \tag{3}$$

where A is the projected contact area, h_c is the contact depth of the indentation, and S is the slope ($\frac{\mathrm{dp}}{\mathrm{dh}}$) of the initial portion of the unloading curve at $h = h_{max}$.

RESULTS AND DISCUSSION

Reduced Modulus

Table 1 shows the reduced modulus and hardness of cured PF resin. The reduced modulus of cured virgin PF was 2.14 GPa. The reduced modulus was increased by the addition of cellulose nanofiber except of CNF-L.

As shown in Table 2, the elastic modulus of cured virgin PF was 9.33 GPa in the glue line, which was prominently higher than that of cured PF at locations either close to the glue line (4.53 GPa) or far from the glue line (5.48 GPa). It is interesting to note that reduced modulus of cured virgin PF in the glue line were much higher than that of cured PF resin.

This could partly be due to a possible extractive effect. Extractives are rich in red oak, ranging from 5.2% in sapwood to 6.3% in heartwood (Gardner *et al.* 1991). When PF glue compounds diffuse into the cell wall, they may become contacted by the extractives. In the glue line, there could be prominently less extractive because there is a higher amount of glue present.

bioresources.com

Table 1. Reduced Modulus (E_r) and Hardness (H) of Cured PF Resin

	E_r (GPa)	H（GPa）
Control	2.14 (0.268)	0.308 (0.0728)
CNC	3.34 (0.361)	0.204 (0.0355)
CNF-L	2.24 (0.118)	0.355 (0.0169)
CNF-C	3.06 (0.311)	0.222 (0.0289)

Note: The numbers in parentheses represent standard deviation (SD)

Tables 2a and 2b show that the addition of CNFs to the PF system resulted in substantial increases in the elastic modulus of cured PF resin. In particular, the largest increase in modulus occurred in PF resin with 3% CNF-C addition. The moduli were 18.5 GPa in the glue line and 17.6 GPa at the location closest to the glue line. The increase in mechanical properties can be attributed to chemical bonding between the methylol groups of the resin and the hydroxyl groups of the cellulose (Singha and Thakur 2008). Higher modulus increases at higher fiber loadings in the glue line are possible because CNFs accumulate in the glue line as fewer fibers penetrate inside the wood structure. Also, when subjected to load, fibers with the reinforced resin act as load carriers, thereby uniformly distributing the stress within the reinforced matrix (Singha and Thakur 2008). The modulus at the location far from the glue line was only 10.5 GPa, much lower than the modulus in the glue line. However, this value was much higher than that of the control sample. This indicates that some of the CNFs, including CNC, were able to penetrate inside the wood microstructure through lumens, vessels, and pits (Kamke and Lee 2007). The CNC particles are much smaller than those of both CNF-C and CNF-L. The average diameter of the CNC was approximately 3.9 nm, and the average length was 148 nm (Meng *et al.* 2014; Wu *et al.* 2013). The CNC particles' rod-like shape makes it difficult for them to penetrate the internal wood microstructure. The reduced modulus of cured CNF reinforced PF in the glue line were much higher than that of cured PF resin on a separate reference sample. This could be due to the accumulation of CNFs in the glue line or lumen as the PF resin could diffuse into wood cell wall.

Also shown in Tables 2a and 2b, the CNFs prominently improved the indentation modulus of the S2 layer. At the location close to the glue line, the modulus of the S2 layer increased 67.1% due to CNC, 45.6% for CNF-L, and 79.0% for CNF-C, in comparison to the control sample. At the location far from the glue line, the modulus of the S2 layer increased much less than at the location close to the glue line.

The addition of cellulose nanofibers improved the modulus of the CCML layer to a much smaller extent. At the location close to the glue line, the modulus of the CCML layer increased by 27.7% for CNC, 11.6% for CNF-L, and 42.9% for CNF-C, in comparison to the control sample. At the location farthest from the glue line, the modulus of the CCML layer increased by 10.6% when using CNC, 8.29% when using CNF-L, and 43.5% when using CNF-C.

Hardness

As shown in Tables 3a and 3b, the hardness of the cured virgin PF was 0.687 GPa in the glue line, which was prominently higher than that of the cured PF at the locations either close to the glue line (0.192 GPa) or far from the glue line (0.188 GPa). This could be attributed to an extractive effect. Extractives, common in red oak, have an impact on hardness similar to that on the modulus.

Table 2a. Reduced Modulus of Interphase in PF Bondlines- Close to Glue Line

	Glue line (GPa)	Close to glue line			
		Distance from glue line (µm)	S2 (GPa)	Inside lumen (GPa)	CCML (GPa)
Control	9.33	31.1	8.38	4.53	6.97
	(1.82)		(1.38)	(1.15)	(0.356)
CNC	14.7	26.6	14.0	13.6	8.90
	(1.50)		(2.08)	(2.14)	(0.992)
CNF-L	16.8	69.6	12.2	9.48	7.78
	(0.817)		(1.67)	(2.45)	(0.0977)
CNF-C	18.5	79.7	15.0	17.6	9.69
	(1.15)		(2.71)	(2.10)	(1.14)

Note: The numbers in parentheses represent standard deviation (SD)

Table 2b. Reduced Modulus of Interphase in PF Bondlines- Far from Glue Line

	Glue Line (GPa)	Far from glue line			
		Distance from glue line (mm)	S2 (GPa)	Inside lumen (GPa)	CCML (GPa)
Control	9.33	0.547	7.31	5.48	6.51
	(1.82)		(0.994)	(0.882)	(0.579)
CNC	14.7	0.602	10.3	9.40	7.20
	(1.50)		(1.93)	(1.79)	(0.710)
CNF-L	16.8	1.00	7.16	7.63	7.05
	(0.817)		(1.12)	(1.17)	(0.528)
CNF-C	18.5	0.395	13.0	10.5	9.34
	(1.15)		(1.93)	(1.08)	(0.260)

Note: The numbers in parentheses represent standard deviation (SD)

Tables 3a and 3b also show that the addition of CNFs to the PF system resulted in a substantial increase in the hardness of the cured PF resin. In the glue line, only PF resin with 3% CNF-L addition had a slight increase in hardness, from 0.687 GPa to 0.894 GPa, compared with that of virgin PF. Its hardness further increased to 0.957 GPa at the location closest to the glue line. The hardness of cured PF with any type of cellulose nano-material addition increased prominently at locations both close to the glue line and far from the glue line, in comparison with that of cured virgin PF at the same locations. However, the hardness was lower than the samples at the glue line, except for in the case of PF resin with a 3% CNF-L addition. For example, the hardness of PF resin with a 3% CNF-C addition was 0.360 GPa at the location far from the glue line. This GPa figure was considerably higher than the 0.188 GPa for the pure resin at the same location, but lower than the 0.687 GPa reading at the glue line. The hardness of cured CNF reinforced PF in the glue line were much higher than that of cured PF resin. This could be due to CNFs accumulate in the glue line or lumen as the PF resin could diffuse into wood cell wall.

At the location close to the glue line, the hardness of the S2 layer increased by 8.92% for CNC, 49.5% for CNF-L, and 47.7% for CNF-C in comparison to the control sample.

At the location far from glue line, the hardness of the S2 layer increased by 49.6% for CNC, 18.0% for CNF-L, and 70.3% for CNF-C compared to that of the control sample.

The hardness of the CCML did not increase with the addition of nano-cellulose materials. The hardness of CCML with a 3% CNF-C addition even decreased by 22.0% at the location close to the glue line and 36.0% at the location far from the glue line in comparison to the control sample. The findings suggest that the PF resin with cellulose nanomaterials was able to improve the modulus but not the hardness of CCML. Further research is needed to explain this.

Table 3a. Hardness of Interphase in PF Bondlines – Close to Glue Line

	Glue line (GPa)	Close to glue line			
		Distance from glue line (µm)	S2 (GPa)	Inside lumen (GPa)	CCML (GPa)
Control	0.687	31.1	0.325	0.192	0.448
	(0.161)		(0.0435)	(0.0102)	(0.0201)
CNC	0.657	26.6	0.354	0.345	0.381
	(0.0245)		(0.0349)	(0.0426)	(0.0662)
CNF-L	0.894	69.6	0.486	0.957	0.349
	(0.0449)		(0.0378)	(0.326)	(0.0363)
CNF-C	0.656	79.7	0.480	0.534	0.446
	(0.0611)		(0.0649)	(0.106)	(0.0423)

Note: The numbers in parentheses represent the standard deviation (SD)

Table 3b. Hardness of Interphase in PF Bondlines- Far from Glue Line

	Glue line (GPa)	Far from glue line			
		Distance (mm)	S2 (GPa)	Inside lumen (GPa)	CCML (GPa)
Control	0.687	0.547	0.256	0.188	0.386
	(0.161)		(0.0335)	(0.0450)	(0.0183)
CNC	0.657	0.602	0.383	0.358	0.365
	(0.0245)		(0.0626)	(0.0647)	(0.0412)
CNF-L	0.894	1.00	0.302	0.313	0.247
	(0.0449)		(0.0312)	(0.0220)	(0.0363)
CNF-C	0.656	0.395	0.436	0.360	0.42
	(0.0611)		(0.0660)	(0.0200)	(0.0471)

Note: The numbers in parentheses represent the standard deviation (SD)

CONCLUSIONS

1. PF resin can improve the modulus and hardness of cell walls (S2 and CCML).

2. The modulus and hardness of cured virgin PF resin inside the lumen were lower than the sample at the glue line due to extractive effects.

3. Cellulose nanomaterials mostly accumulate at the glue lines and have a positive impact on interlocking formation between woods.

4. Cellulose nanomaterials could improve the mechanical properties of adhesives.

5. Cellulose nanomaterials migrate along with resin into the cell lumen, far from the glue line.

ACKNOWLEDGMENTS

REFERENCES CITED

Hunt, C.G., Jakes, J. E., and Grigsby, W. (2010). "Evaluation of adhesive penetration of wood fibre by nanoindentation and microscopy," *10th Pacific Rim Bio-Based Composites Symposium*, 216-226.

Dong, J., Chen, L., Liang, B., Kong, J., Zhao, H., and Liang, F. (2009). "Research and application progress of water-soluble PF," *China Adhesives* 18(10), 37-41.

Gardner, D. J., Generalla, N. C., Gunnells, D. W., and Wolcott, M. P. (1991). "Dynamic wettability of wood," *Langmuir* 7(11), 2498-2502.

Gindl, W., Schoberl, T., and Jeronimidis, G. (2004). "The interphase in phenol-formaldehyde and polymeric methylene diphenyl-di-isocyanate glue lines in wood," *International Journal of Adhesion and Adhesives* 24(4), 279-286.

Jakes, J. E., Yelle, D. Y., Beecher, J. F., Frihart, C. R., and Stone, D. S. (2009). "Characterizing polymeric methylene diphenyl diisocyanate reactions with wood: 2. Nano-indentation," *Wood adhesives 5A – Analytical*, 367-373.

Kaboorani, A., Riedl, B., Blanchet, P., Fellin, M., Hosseinaei, O., and Wang, S. (2012). "Nanocrystalline cellulose (NCC): A renewable nano-material for polyvinyl acetate (PVA) adhesive," *European Polymer Journal* 48(11), 1829-1837.

Kamke, F. A., and Lee, J. N. (2007). "Adhesive penetration in wood – A review," *Wood and Fiber Science* 39, 205-220.

Konnerth, J., and Gindl, W. (2006). "Mechanical characterisation of wood-adhesive interphase cell walls by nanoindentation," *Holzforschung* 60(4), 429-433.

Konnerth, J., Valla, A., and Gindl, W. (2007). "Nanoindentation mapping of a wood-adhesive bond," *Applied Physics A* 88(2), 371-375.

Lee, S., Chang, F., Inoue, S., and Endo, T. (2010). "Increase in enzyme accessibility by generation of nanospace in cell wall supramolecular structure," *Bioresource Technology* 101(19), 7218-7223.

Lee, S., Endo, T., and Kim, N. (2013). "Characteristics of microfibrillated cellulosic fibers and paper sheets from Korean white pine," *Wood Science and Technology* 47(5), 925-937.

Liang, K., Du, G., Hosseinae, O., Wang, S., and Wang, H. (2011). "Mechanical properties of secondary wall and compound corner middle lamella near the phenol–formaldehyde (PF) adhesive bond line measured by nanoindentation," *Advanced Materials Research* 236-238, 1746-1751.

Marra, A. A. (1992). *Technology of Wood Bonding: Principles in Practice*, Van Nostrand Reinhold, US.

Meng, Y., Wang, S., Cai, Z., Young, T.M., Du, G., and Li, Y. (2013). "A novel sample preparation method to avoid embedding medium influence during nanoindentation," *Applied Physics A* 110(3), 361-369.

Meng, Y., Wu, Q., Wang, S., Young, T., Huang, B., and Li, Y. (2014). "Size distribution and geometrical shape of individual cellulose nanocrystals from Switchgrass," *Carbohydrate Polymer* (in review).

Obeng, E. A., Via, B. K., Fasina, O., Auad, M. L., and Jiang, W. (2013). "Cellulose reinforcement of phenol formaldehyde: Characterization and chemometric elucidation," *International Journal of Composite Materials* 3(3), 61-68.

Obersriebnig, M. (2011). "Cross sectional nanoindentation as means of adhesion characterisation at the wood-adhesive bond line," MS thesis, University of Wien, Austria.

Oliver, W. C., and Pharr, G. M. (1992). "An improved technique for determining hardness and elastic modulus using load and displacement sensing indentation experiments," *Journal of Materials Research* 7(6), 1564-1583.

Pizzi, A. (1994). "Advanced wood adhesives technology," Marcel Dekker, Inc.

Salari, A., Tabarsa, T., Khazaeian, A., and Saraeian, A. (2012). "Effect of nanoclay on some applied properties of oriented strandboard (OSB) made from underutilized low quality paulownia (*Paulownia fortunei*) wood," *Journal of Wood Science* 58(6), 513-524.

Singha, A. S., and Thakur, V. K. (2008). "Mechanical properties of natural fiber reinforced polymer composites," *Bulletin of Materials Science* 31(5), 791-799.

Stöckel, F., Konnerth, J., Kantner, W., Moser, J., and Gindl, W. (2010). "Mechanical characterization of adhesives in particle boards by means of nanoindentation," *European Journal of Wood and Wood Products* 68(4), 421-426.

Teixeira, R. S. S., Silva, A. S., Kim, H., Ishikawa, K., Endo, T., Lee, S., and Bon, E. S. P. (2013). "Use of cellobiohydrolase-free cellulose blends for the hydrolysis of microcrystalline cellulose and sugarcane bagasse pretreated by either ball milling or ionic liquid [Emim][Ac]," *Bioresource Technology* 149, 551-555.

Veigel, S., Müller, U., Keckes, J., Obersriebnig, M., and Altmutter, W. G. (2011). "Cellulose nanofibrils as filler for adhesives: Effect on specific fracture energy of solid wood-adhesive bonds," *Cellulose* 18(5), 1227-1237.

Wang, S., and Xing, C. (2010). "Wood adhesives containing reinforced additives for structural engineering products," U.S. Patent Application No. 20100285295.

Wu, Q., Meng, Y., Concha, K., Wang, S., Li, Y., Ma, L., and Fu, S. (2013). "Influence of temperature and humidity on nano-mechanical properties of cellulose nanocrystal films made from switchgrass and cotton," *Industrial Crops and Products* 48, 28-35.

bioresources.com

Wu, Y., Wang, S., Zhou, D., Xing, C., and Zhang, Y. (2009). "Use of nanoindentation and SilviScan to determine the mechanical properties of 10 hardwood species," *Wood and Fiber Science* 41(1), 64-73.

Yan, D., and Li, K. (2013). "Conformability of wood fiber surface determined by AFM indentation," *Journal of Materials Science* 48(1), 322-331.

Zhou, Y., Renneckar, S., Pillai, K. V., Li, Q., Lin, Z., and Church, W. T. (2010). "Layer-by-layer nanoscale bondlines for macroscale adhesion," *BioResources* 5(3), 1530-1541.